On the multiaxial fatigue assessment of complex three-dimensional stress concentrators

R. Louks [a], B. Gerin [b], J. Draper [c], H. Askes [a], L. Susmel [a,*]

[a] Department of Civil and Structural Engineering, The University of Sheffield, Sheffield S1 3JD, United Kingdom
[b] Arts et Métiers ParisTech, CER Angers – Laboratoire LAMPA, 2 Bd du Ronceray, 49035 Angers Cedex 1, France
[c] Safe Technology Limited, Willis House, Peel Street, Sheffield S10 2PQ, United Kingdom

ABSTRACT

This paper assesses and quantifies the detrimental effects of complex tri-dimensional notches subjected to uniaxial and multiaxial fatigue loading. A number of experimental results taken from the technical literature and generated by testing specimens containing complex geometrical features were reanalysed using a critical distance/plane method. The investigated notched samples were tested under uniaxial and multiaxial constant amplitude load histories, considering also the effects of non-zero mean stresses as well as non-proportional loading. The common feature of the considered notched geometries was that the position of the critical location changed as the degree of multiaxiality of the applied loading varied. The relevant linear-elastic stress fields in the vicinity of the crack initiation points were calculated by the Finite Element method and subsequently post-processed using the Modified Wöhler Curve Method in conjunction with the Theory of Critical Distances (the latter theory being applied in the form of the Point Method). This validation exercise confirms the accuracy and reliability of our multiaxial fatigue life assessment technique, which can be efficiently used in situations of practical interest by directly post-processing the relevant linear-elastic stress fields calculated with commercial Finite Element software packages.

1. Introduction

Towards the end of the industrial revolution, it was first noticed that metallic components could become *tired* or *fatigued*. In the 1830s, Wilhelm Albert [1] built the first fatigue test machine and published the first fatigue results, testing actual components rather than just the material. In the 1860s, August Wöhler [2] published his results of fatigue testing on railway axles, tests which were carried out *in situ* where rail carriages were in service. Throughout his investigation he discovered that stress amplitudes are the most important parameter for fatigue life assessment and that a tensile mean stress also has a detrimental influence. Wöhler was the first to take note of the phenomenon of crack propagation, noticing that hairline cracks, in particular those that are radial on the train axels, after years in service would grow, eventually resulting in the breakage of the axles themselves. A few years later Ludwig Spangenberg [3] plotted Wöhler's fatigue data in graphical form but he used a linear scale for the abscissa and ordinates. Subsequently Basquin showed the fatigue results on a log–log graph which is the fundamental layout of a *Wöhler Curve* as used up till recent advances which further improve the accuracy [4]. In 2002, a bi-parametric Wöhler curve was proposed and successfully tested for the multiaxial fatigue assessment and later referred to as the Modified Wöhler Curve Method (MWCM) [5]. As to the multiaxial fatigue issue, it is worth observing here that, starting from the pioneering work done by Gough back in the 1940s [6], a tremendous effort has been made by the scientific community to propose reliable criteria suitable for estimating fatigue damage under multiaxial fatigue loading. Amongst the different methods which have been proposed and experimentally validated so far certainly the criteria formalised by Dang Van et al. [7], Papadopoulos [8], Liu [9], Fatemi and Socie [10], and Brown and Miller [11] deserve to be mentioned explicitly.

Although Wöhler noticed a decrease in strength due to the presence of notches, it was the pioneering work carried out by Neuber [12] and Peterson [13] that systematically evaluated the notch effect in fatigue. From a design point of view, Neuber proposed to calculate an effective stress to estimate high-cycle notch fatigue strength by averaging the linear-elastic stresses over a line. Subsequently, Peterson simplified the above approach by suggesting that the effective stress could directly be calculated by simply using the stress at a given distance from the notch apex. The common feature of the above notch fatigue methods is that the effective stress depends on a material characteristic length. These are early examples of the so-called Theory of Critical Distances (TCD). Using concepts

* Corresponding author.
  E-mail address: l.susmel@sheffield.ac.uk (L. Susmel).

of Linear Elastic Fracture Mechanics (LEFM), in recent years such a theory has been reformulated by David Taylor to make it suitable for addressing different structural integrity problems [14].

Following on from the historical review it can be said that much effort has gone into understanding the physics of fatigue, paying particular attention to the detrimental effect of stress raisers [5,14]. Examination of the state of the art suggests that, apart from a few isolated investigations (see, for instance, Refs. [15,16]), so far the notch fatigue issue has been addressed mainly by considering standard stress risers whose detrimental effect could directly be assessed by considering bi-dimensional geometrical configurations, the crack initiation locations being unambiguously known *a priori*. On the contrary, real components often contain complex three-dimensional (3D) geometrical features, where the position of the hot-spots is not always obvious, especially in the presence of very complex multiaxial fatigue load histories [16]. It is reported that current methods used to assess the effects of 3D stress concentrators often predict conservative results, typically by a factor of 2 [15]. This obviously results in components which are heavier than required, unnecessarily increasing the material usage and the associated manufacturing costs.

In this complex scenario, by reanalysing a large number of experimental results taken from the literature, the present paper aims to investigate the accuracy of the MWCM [5], applied along with the TCD [14], in estimating fatigue strength in the presence of complex 3D stress concentrators subjected to uniaxial and multiaxial fatigue loading.

2. Fundamentals of the Modified Wöhler Curve Method applied with the Point Method

The MWCM is a bi-parametrical critical plane approach [5] designed to estimate both high-cycle fatigue strength and finite lifetime of engineering materials subjected to in-service multiaxial fatigue loading. The MWCM postulates that, independently from the degree of multiaxiality and non-proportionality of the applied loading path, Stage I fatigue cracks (Fig. 1a) initiate on those

material planes experiencing the maximum shear stress amplitude, τ_a. In this context, the orientation of the critical plane is recommended here to be determined through the Shear Stress-Maximum Variance Method (τ-MVM) [17,18]. In more detail, contrary to other existing techniques such as the Longest Chord [19], Longest Projection [20], Minimum Circumscribed Circle [21], and Minimum Circumscribed Ellipse Method [22–25], the τ-MVM postulates that the orientation of the critical plane can be determined by locating those material planes containing the direction experiencing the maximum variance of the resolved shear stress. This approach is seen to be very efficient from a numerical point of view, since, as soon as the variance and co-variance terms characterising the load history under investigation are known, the computational time required to reach convergence is not affected by the length of the stress signal being post-processed [17] – the Reader is referred to Ref. [17] for the mathematical formalisation of the τ-MVM, whereas its accuracy in estimating the orientation of Stage I planes is discussed in Ref. [18] in great detail.

Turning back to the fatigue damage model on which the MWCM is based, also the stress component perpendicular to the critical plane is assumed to play an important role in the fatigue cracking process. In particular, the hypothesis is that Stage I cracks always initiate on those material planes experiencing the maximum shear [26–28], whereas their subsequent propagation is influenced by the normal stress which cyclically opens and closes the microcracks themselves – see Refs. [29,30] and Fig. 1a. The combined effect of the above two stress components relative to the critical plane can be taken into account through the following stress ratio [30]:

$$\rho_{eff} = \frac{m \cdot \sigma_{n,m} + \sigma_{n,a}}{\tau_a} \tag{1}$$

In the above definition, $\sigma_{n,m}$ and $\sigma_{n,a}$ are the mean value and the amplitude of the stress normal to the critical plane, respectively. The mean stress sensitivity index m instead is assumed to be a material property, ranging from 0 to 1, suitable for quantifying the material sensitivity to superimposed static stresses [5,30].
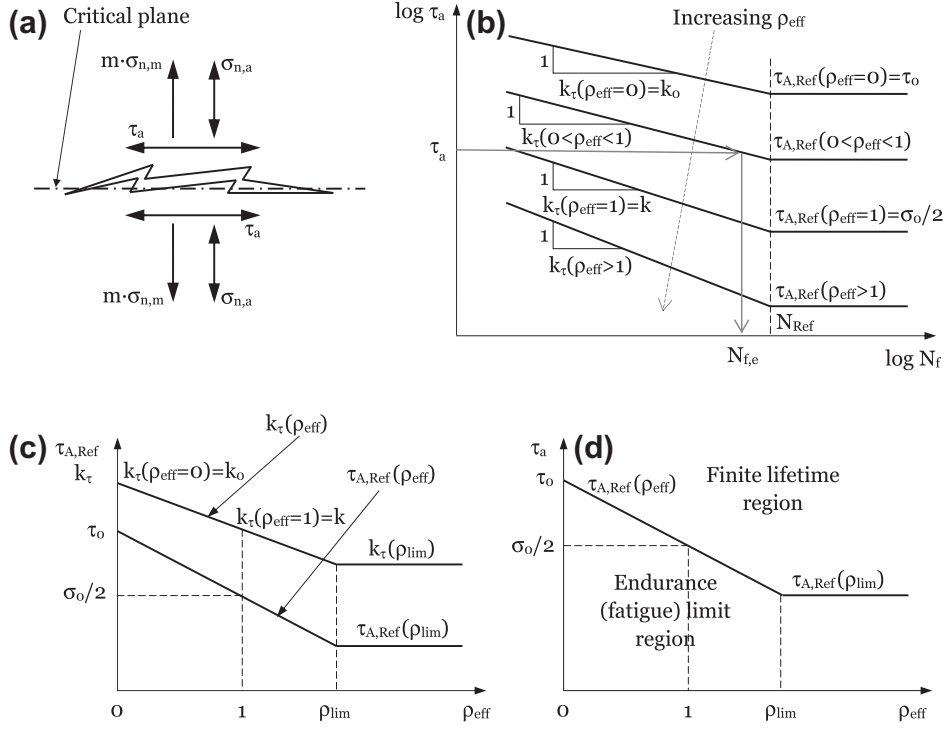
Fig. 1. Fatigue damage model (a), modified Wöhler diagram (b), MWCM's calibration functions (c), and multiaxial endurance (fatigue) limit region defined according to the MWCM (d).

Ratio ρ_{eff} is seen to be sensitive not only to the presence of non-zero mean stresses, but also to the degree of multiaxiality and non-proportionality of the applied load history [5].

According to the MWCM, fatigue damage can be quantified through modified Wöhler diagrams plotting the shear stress amplitude relative to the critical plane, τ_a, against the number of cycles to failure, N_f (Fig. 1b). As shown in the schematic chart of Fig. 1b, it is assumed that, for a given material, the modified Wöhler curves shift downwards as the ratio ρ_{eff} increases, the limit value for such a stress ratio being [5,27,30]:

$$\rho_{eff} \leqslant \rho_{lim} = \frac{\tau_0}{2\tau_0 - \sigma_0} \tag{2}$$

where σ_0 and τ_0 are the endurance limits extrapolated at N_{Ref} cycles to failure under fully-reversed uniaxial ($\rho_{eff} = 1$) and torsional ($\rho_{eff} = 0$) fatigue loading, respectively.

In situations of practical interest, solely the fatigue curves generated under fully-reversed uniaxial and torsional fatigue loading are available, so that the position of any other modified Wöhler curve can be directly estimated through the following calibration functions [26,27]:

$$k_\tau(\rho_{eff}) = (k - k_0) \cdot \rho_{eff} + k_0 \quad (\text{for } \rho_{eff} \leqslant \rho_{lim}) \tag{3}$$

$$\tau_{A,Ref}(\rho_{eff}) = \left(\frac{\sigma_0}{2} - \tau_0\right) \cdot \rho_{eff} + \tau_0 \quad (\text{for } \rho_{eff} \leqslant \rho_{lim}) \tag{4}$$

where, given the modified Wöhler curve, $k_\tau(\rho_{eff})$ is its negative inverse slope and $\tau_{A,Ref}(\rho_{eff})$ is the reference shear stress at N_{Ref} cycles to failure (Fig. 1b). In Eq. (3) k and k_0 denote the inverse slope of the fatigue curves experimentally generated under fully-reversed uniaxial ($\rho_{eff} = 1$) and torsional ($\rho_{eff} = 0$) fatigue loading, respectively. Eqs. (3) and (4) are also plotted in Fig. 1c: such a schematic chart shows that, when $\rho_{eff} > \rho_{lim}$, $\tau_{A,Ref}(\rho_{eff})$ is suggested as being taken invariably equal to $\tau_{A,Ref}(\rho_{lim})$ and $k_\tau(\rho_{eff})$ to $k_\tau(\rho_{lim})$ [5]. This hypothesis was formed in order to model more accurately the material fatigue behaviour observed under large values of ratio ρ_{eff}, by simultaneously reducing the intrinsic level of conservatism charac-

terising the critical plane approach when used to address such situations [31].

Finally, as soon as the modified Wöhler curve is estimated for the ρ_{eff} value being assessed, the number of cycles to failure, $N_{f,e}$, can directly be predicted through the amplitude of the shear stress relative to the critical plane, τ_a, by using the following trivial relationship [27] (see also Fig. 1b):

$$N_{f,e} = N_{Ref} \cdot \left[\frac{\tau_{A,Ref}(\rho_{eff})}{\tau_a}\right]^{k_\tau(\rho_{eff})} \tag{5}$$

According to the modified Wöhler diagram of Fig. 1b, the MWCM can also be used to perform the high-cycle fatigue assessment [5]. In particular, it is straightforward to observe that a material is assumed to be at its endurance (fatigue) limit when the following condition is satisfied [26]:

$$\tau_a \leqslant \tau_{A,Ref}(\rho_{eff}) = \left(\frac{\sigma_0}{2} - \tau_0\right) \cdot \rho_{eff} + \tau_0 \tag{6}$$

This condition is also summarised in the τ_a vs. ρ_{eff} diagram of Fig. 1d. As to this schematic chart, it is worth observing here that, for the same reasons as those discussed above, when ρ_{eff} is larger than ρ_{lim}, $\tau_{A,Ref}(\rho_{eff})$ is suggested as being taken equal to $\tau_{A,Ref}(\rho_{lim})$ [30]. By re-arranging Eq. (6), it is also possible to define an equivalent shear stress amplitude, $\tau_{A,eq}$, as follows:

$$\tau_{A,eq} = \tau_a + \left(\tau_0 - \frac{\sigma_0}{2}\right) \cdot \rho_{eff} \leqslant \tau_0 \tag{7}$$

From a fatigue design point of view, the above effective stress can be directly used to calculate an appropriate high-cycle multiaxial fatigue safety factor, i.e.:

$$\nu_{HSF} = \frac{\tau_0}{\tau_{A,eq}} \geqslant 1 \tag{8}$$

The MWCM can also be employed to design notched components against fatigue, either in terms of nominal stresses [27] or along with the TCD [32–35].

The TCD can be formalised in different ways which include the Point (PM), the Line (LM), the Area (AM), and the Volume Method (VM). The PM is the simplest approach to be used in situations of practical interest: according to Peterson's idea [13], the PM postulates that fatigue strength can directly be estimated by using the stress state at a given distance from the apex of the stress raiser being assessed [14].

In order to apply correctly the MWCM in conjunction with the PM, the first problem to be addressed is the determination of the so-called *focus path*, the way of defining it to design complex 3D geometrical features against fatigue being investigated in great detail in the next section. Consider then a mechanical component subjected to a complex system of time-variable forces/moments and assume that the crack initiation point is known *a priori*, i.e. point A in Fig. 2a and b: according to these figures, the focus path is assumed to emanate from point A and it is perpendicular to the surface at the crack initiation point itself [5,34]. In the presence of sharp corners (i.e., zero-radius notches), the focus path is recommended as being taken coincident with the notch bisector [5].

To perform the high-cycle fatigue assessment of the component sketched in Fig. 2a, the linear-elastic stress state to be post-processed is the one acting on that point positioned, along the focus path, at a distance from the assumed crack initiation location equal to $L/2$ (Fig. 2a), where the high-cycle fatigue critical distance is defined as [14,32,33].

$$L = \frac{1}{\pi}\left(\frac{\Delta K_{th}}{\Delta\sigma_0}\right)^2 \tag{9}$$

In the above definition, ΔK_{th} is the range of the threshold value of the stress intensity factor, whereas $\Delta\sigma_0$ is the range of the unnotched fatigue (endurance) limit. According to the MWCM the notched component being designed is then assumed to be at its fatigue (endurance) limit when condition (6) is assured, τ_a, $\sigma_{n,m}$, and
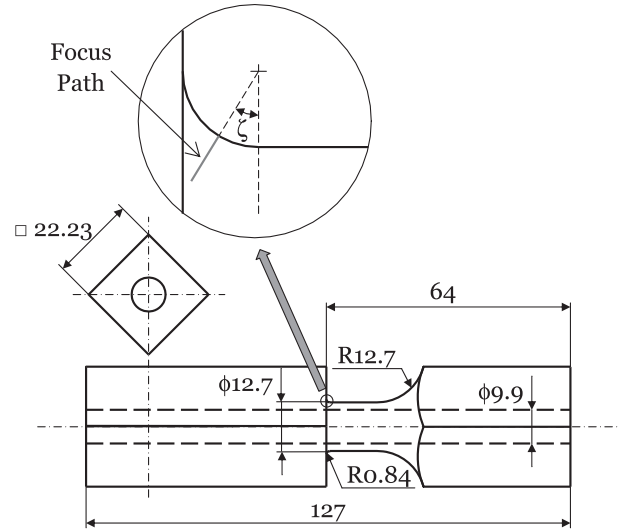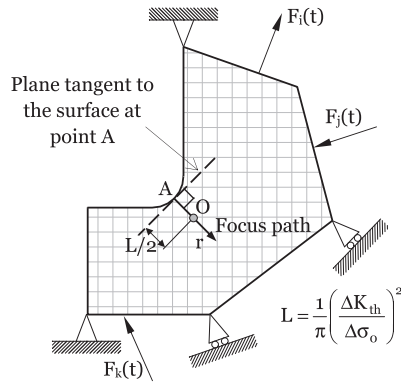

Fig. 3. Specimens with fillet of steel S65A tested by Gough [6] and angle ζ defining the orientation of the focus path.
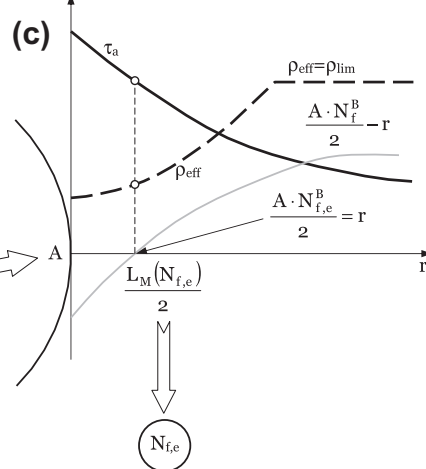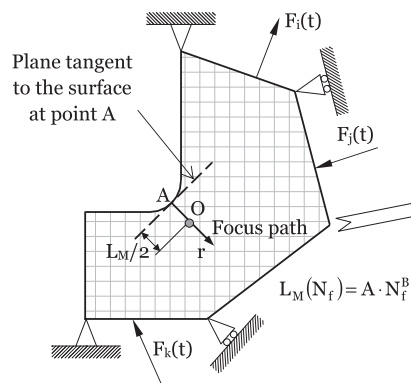

Fig. 2. Definition of the focus path (a and b) and in-field procedure to estimate finite lifetime (c).

$\sigma_{n,a}$ being calculated by post-processing the linear-elastic stress state determined at a distance from the crack initiation point equal to $L/2$ (i.e., at point O in Fig. 2a). As to definition (9), it is worth observing here also that L is recommended to be always estimated through fatigue properties (i.e., $\Delta\sigma_0$ and ΔK_{th}) experimentally determined under fully-reversed loading, the mean stress effect being directly taken into account by the MWCM itself [33].

The MWCM can be applied together with the PM also to estimate finite lifetime, provided that the critical distance increases as the number of cycles to failure, N_f, decreases, i.e. [34,36]:

$$L_M(N_f) = A \cdot N_f^B \tag{10}$$

In the above definition, A and B are material fatigue properties to be estimated from the fully-reversed unnotched uniaxial fatigue curve as well as from a fully-reversed uniaxial notch fatigue curve generated by testing samples containing a known geometrical feature [36]. It is worth recalling here that the above fatigue curves are always recommended as being experimentally generated under fully-reversed loading since the detrimental effect of non-zero mean stresses is directly taken into account by the MWCM itself [34,35].

Table 1
Safety factor, ν_{HSF}, calculated according to the MWCM applied along with the PM for the samples with fillet of S65A tested by Gough [6] as the orientation of the focus path varies – see also Fig. 3.

Loading path	ζ (°)	τ_a (MPa)	$\sigma_{n,a}$ (MPa)	$\sigma_{n,m}$ (MPa)	ρ_{eff}	$\tau_{A,eq}$ (MPa)	ν_{HCF}	Error (%)
Fully-reversed bending	0	294.2	302.2	0.0	1.027	375.1	0.99	1.2
	22.5	325.0	345.4	0.0	1.063	408.7	0.91	10.3
	45	231.0	245.2	0.0	1.061	314.6	1.18	−15.1
	67.5	112.3	118.4	0.0	1.054	195.3	1.90	−47.3
Fully-reversed torsion	0	335.6	0.0	0.0	0	335.6	1.10	−9.4
	22.5	361.7	0.0	0.0	0	361.7	1.02	−2.4
	45	312.0	0.0	0.0	0	312.0	1.19	−15.8
	67.5	236.0	0.0	0.0	0	236.0	1.57	−36.3

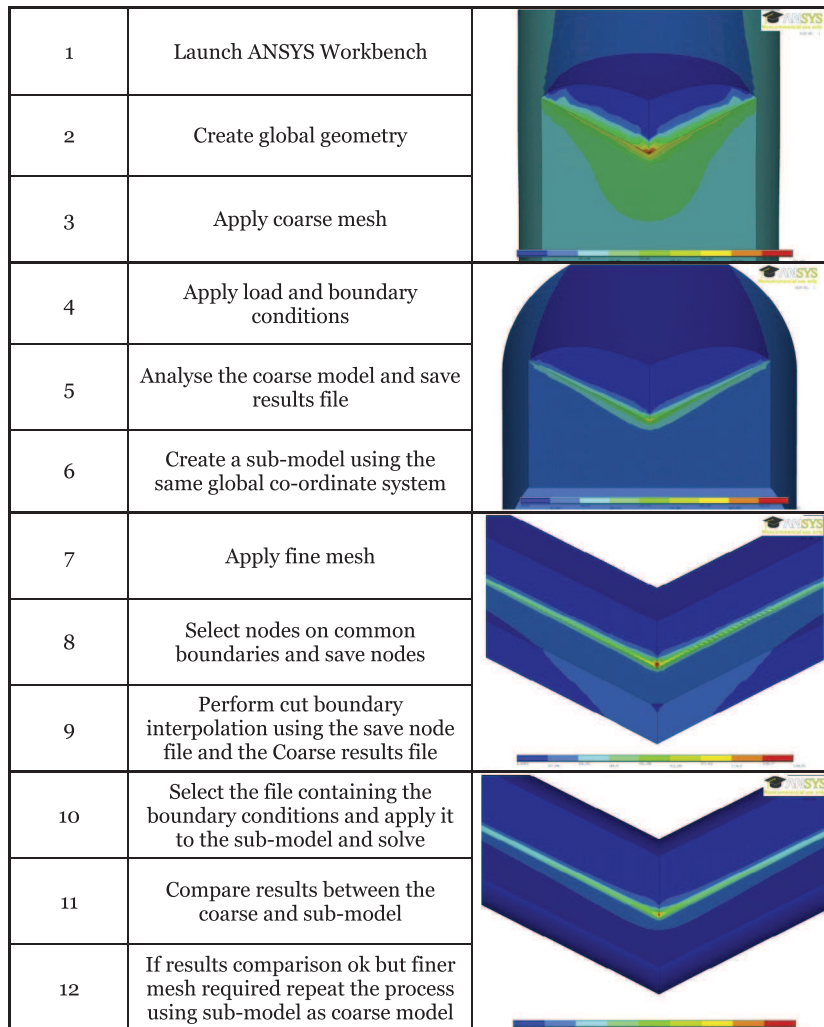|		
1	Launch ANSYS Workbench	
2	Create global geometry	
3	Apply coarse mesh	
4	Apply load and boundary conditions	
5	Analyse the coarse model and save results file	
6	Create a sub-model using the same global co-ordinate system	
7	Apply fine mesh	
8	Select nodes on common boundaries and save nodes	
9	Perform cut boundary interpolation using the save node file and the Coarse results file	
10	Select the file containing the boundary conditions and apply it to the sub-model and solve	
11	Compare results between the coarse and sub-model	
12	If results comparison ok but finer mesh required repeat the process using sub-model as coarse model	

Fig. 4. Solid-to-solid sub-modelling procedure followed to perform the stress analysis using commercial FE software ANSYS® – see Fig. 11 for the details of the notched geometry considered in the flowchart.

The assumption that, in the finite lifetime regime, the critical distance value varies with N_f is due to the fact that the size of the plastic region in the vicinity of the notch tip is seen to increase as the magnitude of the applied cyclic loading increases. Accordingly, the cyclic plastic behaviour of ductile metals is accommodated into the linear-elastic PM framework by forming the hypothesis that the size of the process zone (which in turn sets the magnitude of L_M) increases as the amplitude of the local cyclic stress increases [5,34,36].

After defining the focus path as briefly discussed above (see Fig. 2b), both τ_a and ρ_{eff} have to be determined along the focus path itself. These two stress quantities can then be plotted against distance r as schematically shown in Fig. 2c. Through both τ_a and ρ_{eff}, the corresponding Modified Wöhler curve can then be estimated, at any distance r from the assumed crack initiation location, through Eqs. (3) and (4), after which the resulting number of cycles

to failure, $N_{f,e}$, is predicted according to Eq. (5). Finally, the notched component is assumed to fail at the number of cycles to failure as estimated by the following condition (Fig. 2c) [36]:

$$\frac{L_M(N_f)}{2} - r = 0 \tag{11}$$

3. On the determination of the focus path to design complex/3D stress concentrators against fatigue

A complex 3D geometrical stress raiser produces multiaxial stress fields in the material around such a feature, the stress gradient decreasing in all directions from the point experiencing the largest stress state (i.e., the so-called hot-spot). Further, given the geometry of the component, the position of the hot-spot can shift depending on the degree of multiaxiality and non-proportionality
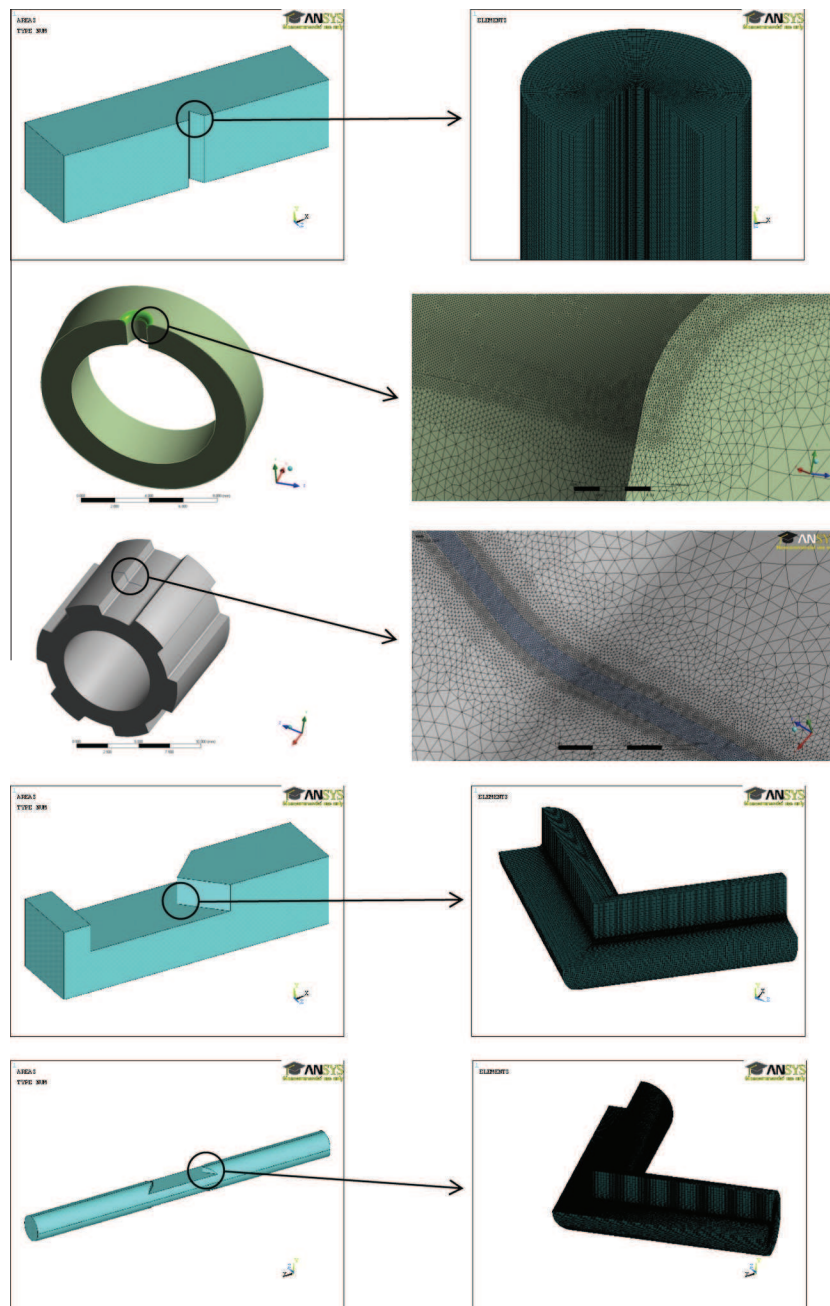

Fig. 5. Finite element models of the investigated notched specimens (the technical drawings of the specimens are reported in Figs. 6 and 8–11).

of the loading path being applied. In this scenario, as briefly mentioned in the previous section, the focus path is assumed to emanate from the crack initiation point, where fatigue cracks cannot necessarily initiate at those superficial points experiencing the largest stress magnitude. This implies that to apply our design procedure in the presence of complex 3D stress concentrators subjected to complex multiaxial load histories, fatigue damage has to be estimated by considering several potential focus paths to find the one which experiences the maximum fatigue damage extent.

In order to discuss the problem of estimating the position of the focus path in detail, we consider the classic experimental results generated by Gough [6] by testing, under fully-reversed pure bending and pure torsion, the samples with fillet sketched in Fig. 3. The above specimens were made of S65A, a high-strength steel having the following mechanical properties: σ_{UTS} = 1000 MPa, σ_y = 946.3 MPa, σ_0 = 583.5 MPa, τ_0 = 370.5 MPa, critical distance L being estimated to be equal to 0.056 mm [33].

Table 1 summarises the safety factors – see Definition (8) – calculated according to the MWCM applied in conjunction with the PM as the orientation of the adopted focus path varies, angle ζ being defined as shown in Fig. 3. The above Table also reports the high-cycle fatigue error calculated as follows:

$$\text{Error} = \frac{\tau_{A,eq} - \tau_0}{\tau_0} \ (\%) \tag{12}$$

The above Table makes it evident that fatigue damage is maximised along paths having ζ angle equal to about 22.5°, this holding true both under fully-reversed bending and fully-reversed torsion. As to the overall accuracy of the TCD based methods, it is worth observing here that such approaches are seen to be capable of high-cycle fatigue estimates falling within an error interval equal to about ±20% [14,37,38]. It is generally believed that one cannot distinguish between an error of 20% and an error of 0% due to the well-known problems which are usually encountered during testing as well as during the numerical analyses [37], the local material morphology playing a role of primary importance in defining the physiological level of scattering that are typically found in fatigue results [5]. According to the above considerations, in Gough's samples (Fig. 3) fatigue cracks are expected to initiate, within the fillet, in a material region close to the junction between the fillet itself and the net section of the specimens, i.e., in a region characterised by an error in the estimates of about ±20%. This explains the reason why in Ref. [33] accurate estimates were obtained by forming the engineering hypothesis that in shafts with fillet fatigue cracks initiate at the toe of the fillet itself. The validity of the above idea is also supported by the cracking behaviour observed by Gough himself, who affirmed [6] that "*nearly all the specimens failed similarly, by a transverse crack situated at the junction of the fillet with the parallel central portion of the test-piece or slightly removed from that junction and within the fillet*".

In the specimens with fillet tested by Gough [6], fatigue cracks were seen to initiate mainly at the fillet end, even though the points experiencing the maximum stress (calculated according to either the maximum principal stress or von Mises criterion) are characterised by a ζ angle equal to about 18° (this holding true under both pure bending and pure torsion). This experimental evidence further confirms that, as briefly mentioned above, in the presence of complex 3D geometries fatigue cracks can also emanate from materials points which are not subjected to the maximum stress magnitude.

In summary, from a design point of view the safest way to perform the fatigue assessment of complex 3D notched components subjected to complex multiaxial load histories is by searching for that focus path which experiences the largest fatigue damage extent estimated according to the MWCM, the stress analysis being performed in terms of the PM.

4. Validation by experimental data

In order to evaluate the overall reliability of the design methodology briefly described in the previous sections, in what follows the accuracy of our approach will be checked against a number of experimental results generated by testing complex/3D notches under both uniaxial and multiaxial fatigue loading. The experimental results are reanalysed by grouping the investigated geometries according to their typology as well as to the degree of multiaxiality of the applied load history.

4.1. Stress and strength analysis

To post-process correctly the results collected from the technical literature, the required linear-elastic stress fields were determined by using commercial FE software ANSYS®. The FE models were solved by assuming a linear-elastic behaviour for the material being investigated. In the vicinity of the potential crack initiation locations, the mesh density was gradually increased until convergence occurred, this process resulting in elements having, in the
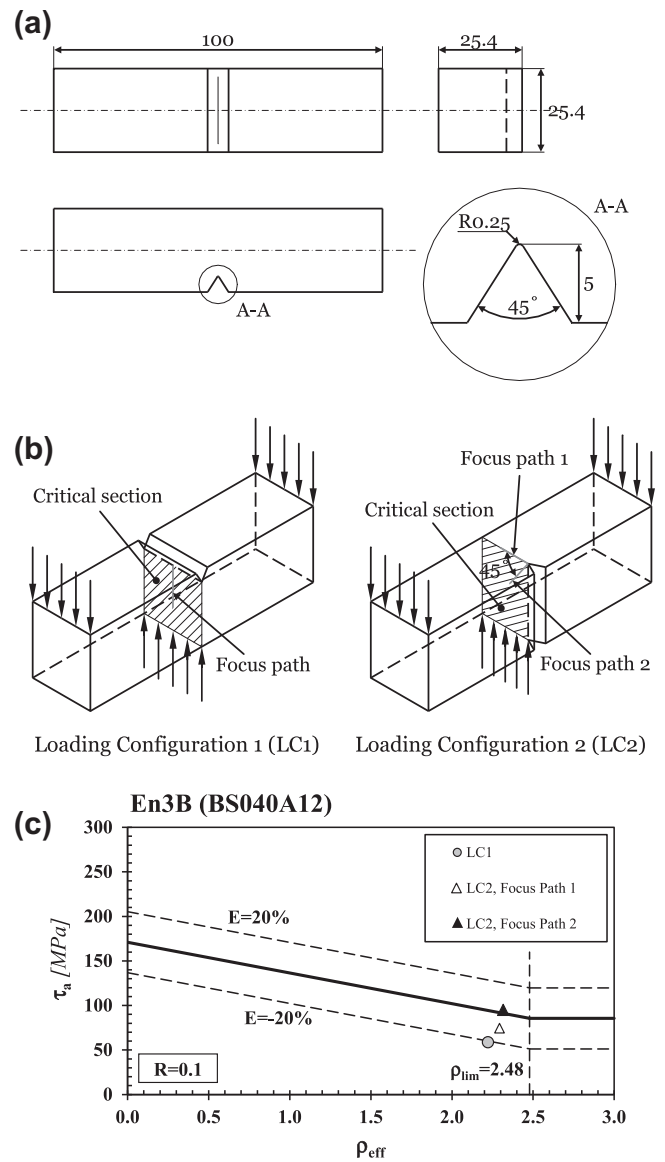

Fig. 6. Geometry of the V-notched samples loaded in three-point bending (a) and loading configurations (b) [15,41], high-cycle fatigue strength estimated according to the MWCM (c).

process zone, a size of the order of 2.5 µm. Due to the large number of elements used to estimate the stress fields in the critical regions, solutions were calculated by following a conventional solid-to-solid sub-modelling procedure (Fig. 4). For those results generated under biaxial loading, the relevant linear-elastic stress fields were numerically determined under simple uniaxial loading (i.e., either tension or bending) as well as under simple torsion, the total stress fields being subsequently determined by taking full advantage of the superposition principle (obviously, paying attention not to lose the synchronisation amongst the different nominal stress components) [5]. A number of screenshots showing the FE models which were solved using commercial software ANSYS® are reported in Fig. 5, the associated stress and strength analysis issues being discussed in what follows.

The stress fields in the vicinity of the micro-hole tested by Endo [39] and having diameter of 500 µm (see Section 4.3) were instead determined by using the classic solution proposed by Kirsch for plane stress distributions [40].

Both high-cycle fatigue strength and finite lifetime were estimated by using our software Multi-FEAST© (www.multi-feast.com) to post-process directly the stress fields determined as briefly described above. Multi-FEAST is a post-processor which works by coupling three pieces of information: the stress states or fields at the critical locations, the load history that the component is being subjected to, and the fatigue response of the material. The stress state can be taken from any finite element package and the user can include the sub-surface stresses around the notch or geometrical feature. Alternatively, the relevant stress fields can be determined from classical solid mechanics analytical solutions (for instance, by taking full advantage of either beam theory or the classical equations suitable for describing stress fields in the vicinity of stress raisers). Similarly, the load history can be defined either

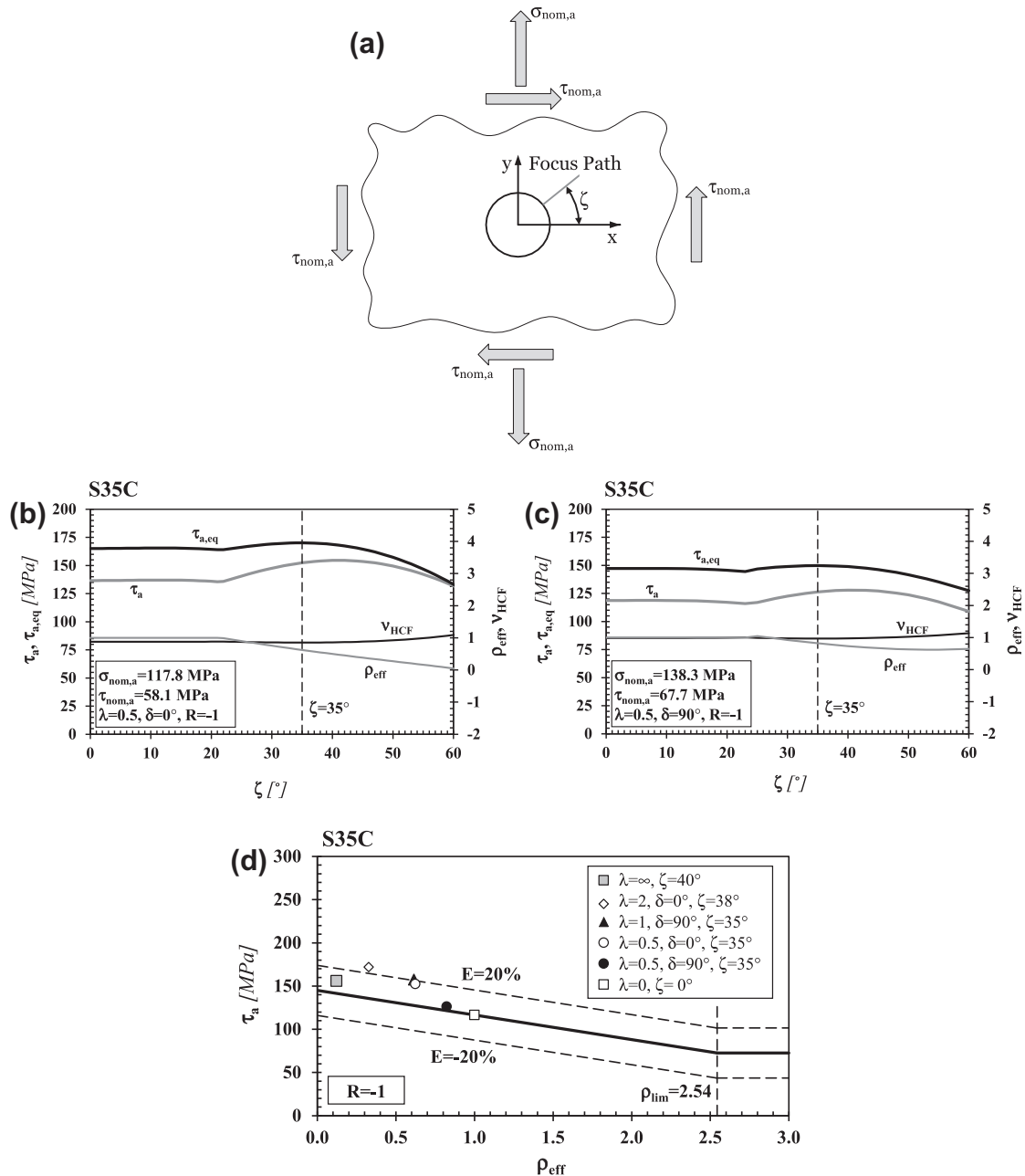**Fig. 7.** Micro-holes subjected to combined axial loading and torsion [39] (a), τ_a, $\tau_{a,eq}$, ρ_{eff}, ν_{HCF} vs. angle ζ diagrams under in-phase (b) and out-of-phase loading (c), high-cycle fatigue strength estimated according to the MWCM (d).

analytically, a simple sinusoidal loading for example, or constructed from a combination of varying loads or from load signals gathered experimentally using transducers or strain gauges attached to the
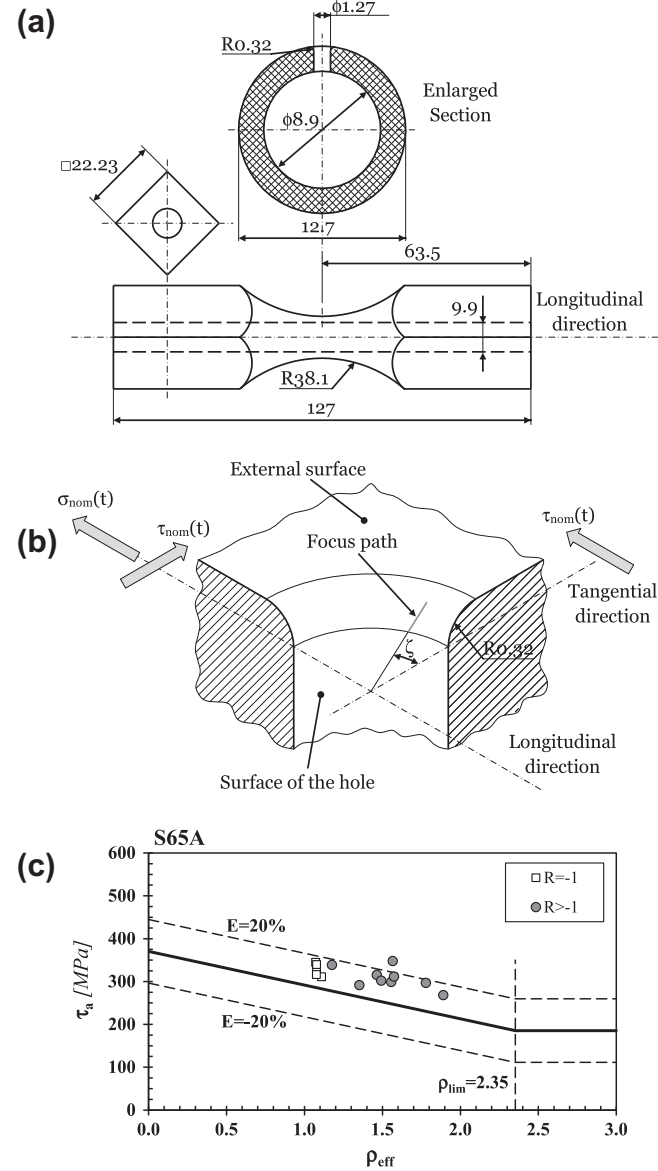
component surface. Indeed, any experimentally determined stresses or strains can be used which opens the possibilities up to data collected by photoelastic, thermoelastic or digitial image correlation methods. Finally, to estimate fatigue damage, the appropriate material properties can either be determined from experiments on the material of interest, extracted from a database, or estimated using *ad hoc* empirical rules.

4.2. V-notched samples loaded in three-point bending

The first geometry which was investigated to check the accuracy of our approach in designing 3D notches against fatigue is a square section beam with a through V-notch on one side (see Fig. 6a) [15,41]. The samples were made of En3B (BS040A12) which is a low-carbon steel having the following mechanical/fatigue properties [32]: ultimate tensile strength $\sigma_{UTS} = 410$ MPa, fully reversed uniaxial fatigue limit $\sigma_0 = 273$ MPa, fully reversed torsional fatigue limit $\tau_0 = 171$ MPa, critical distance $L = 0.2$ mm and mean stress sensitivity index $m = 1$. The above samples were cyclically loaded in three-point bending under a load ratio R equal to 0.1. Two loading configurations were considered, i.e. by applying the force perpendicular (Fig. 6b) and parallel (Fig. 6c) to the notch. Due to the simplicity of the geometry, it was straight-forward to guess the position of the crack initiation locations. In particular, when the samples were loaded with the force being perpendicular to the notch (Loading Configuration 1, LC1), the focus path was assumed to emanate from the notch tip at the mid-section of the samples, that is, at that specimen section experiencing the largest degree of triaxiality (Fig. 6b). Under Loading Configuration 2 (LC2) the focus path was assumed to emanate from the notch tip at the surface by considering two possible directions: Focus Path 1 was taken coincident with the notch bisector belonging to the upper surface, whereas Focus Path 2 was assumed instead to be at 45° to the upper surface (Fig. 6c). The observed cracking behaviour [29] confirms the validity of the hypothesis formed to define the position of the crack initiation locations.

The τ_a vs. ρ_{eff} diagram of Fig. 6d shows the overall accuracy obtained by applying the MWCM along the PM to estimate the high-cycle fatigue strength of the samples sketched in Fig. 6a: such a chart makes it evident that our design approach was capable of estimating the high-cycle fatigue strength within the usual error interval of ±20%. As to Loading Configuration 2, it is worth observing here that the focus path resulting in the largest damage extent is seen to be Focus Path 2. This fully agrees with the observed cracking behaviour: cracks initiated, from the upper surface, at the tip of the notch, the crack front propagating inward along a direction at about 45° to the surface itself [41].

To conclude, it is interesting to notice that the predictions made by Bellett et al. [15,41] by applying the TCD along with the

Fig. 8. Macro-holes subjected to combined bending and torsion [6], focus path and definition of angle ζ (b), high-cycle fatigue strength estimated according to the MWCM (d) – see also Table 2.

Table 2
Accuracy in estimating the experimental results generated by Gough by testing holed samples [6] – see also Fig. 8.

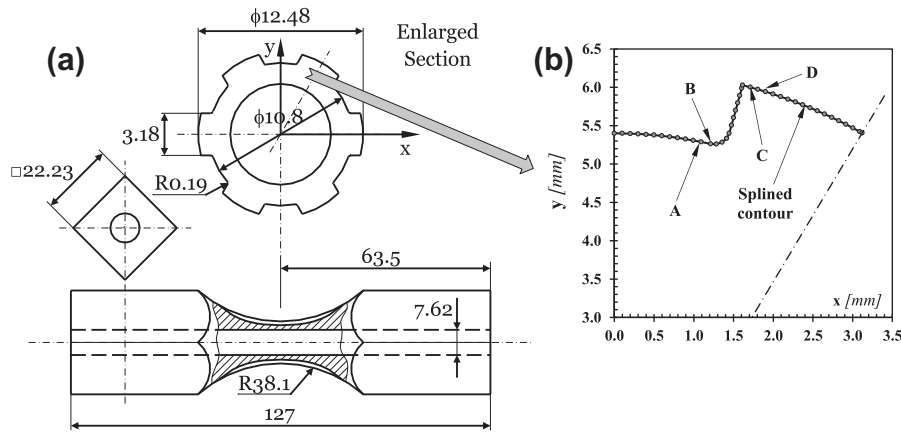| $\sigma_{nom,a}$ (MPa)	$\sigma_{nom,m}$ (MPa)	$\tau_{nom,a}$ (MPa)	$\tau_{nom,m}$ (MPa)	τ_a (MPa)	ρ_{eff}	ζ (°)	Error (%)
259.4	0	0	0	339.6	1.078	0.0	14.6
237.8	266.3	0	0	311.3	1.574	0.0	17.5
259.4	0	0	169.8	338.7	1.177	2.9	16.4
236.2	266.3	0	169.8	347.7	1.566	2.9	27.1
0	0	180.6	0	310.7	1.110	42.9	7.5
0	266.3	169.8	0	291.5	1.352	40.0	7.4
0	0	173.7	169.8	298.8	1.557	42.9	13.7
0	266.3	172.9	169.8	296.8	1.779	40.0	17.9
174.5	0	115.8	0	329.7	1.078	25.8	11.9
159	266.3	106.5	0	301.8	1.492	25.8	13.2
166.8	0	111.2	169.8	315.4	1.464	28.6	16.2
142	266.3	94.2	169.8	268.2	1.891	25.8	12.6
219.2	0	61.8	0	316.1	1.077	14.3	8.2
86.5	0	171.4	0	344.9	1.072	34.3	15.9

Fig. 9. Splined shaft subjected to combined bending and torsion [6] (a), origins of the explored focus paths (b), high-cycle fatigue strength estimated according to the MWCM (c) – see also Table 3.

Table 3
Accuracy in estimating the experimental results generated by Gough by testing splined shafts [6] – see also Fig. 9.

$\sigma_{nom,a}$ (MPa)	$\sigma_{nom,m}$ (MPa)	$\tau_{nom,a}$ (MPa)	$\tau_{nom,m}$ (MPa)	τ_a (MPa)	ρ_{eff}	Critical location[a]	Error (%)
563.6	0	0	0	311.0	0.971	C	4.6
537.3	266.3	0	0	296.5	1.169	C	4.9
534.2	0	0	169.8	287.3	1.128	D	1.5
540.4	266.3	0	169.8	290.7	1.328	D	6.7
0	0	185.3	0	281.9	0.014	A	−23.6
0	266.3	188.4	0	286.6	0.374	A	−14.7
0	0	177.6	169.8	270.1	0.020	A	−26.7
0	266.3	173.7	169.8	264.3	0.406	A	−20.0
264	0	176	0	296.6	0.443	A	−10.5
247	266.3	163.7	0	253.8	0.879	B	−12.8
253.2	0	168.3	169.8	283.8	0.605	A	−10.6
250.1	266.3	166.8	169.8	281.1	0.629	A	−10.8
501.8	0	142	0	324.6	0.769	A	4.0
95.7	0	189.9	0	291.2	0.165	A	−17.9

[a] See Fig. 9b for the definition of the critical locations.

maximum principal stress criterion resulted in a very large degree of conservatism. It is the authors' opinion that such a level of conservatism may be ascribed simply to the fact that, contrary to the MWCM, the maximum principal stress alone is not capable of correctly taking into account the actual degree of multiaxiality of the local stress fields.

4.3. Holed samples subjected to biaxial loading

In order to investigate the accuracy of our approach in modelling the detrimental effect of very small stress concentrators, it was attempted to be used to estimate the high-cycle fatigue strength of cylindrical samples containing holes having diameter/

depth of 500 μm and subjected to combined tension and torsion (Fig. 7a) [39]. Steel S35C investigated by Endo and Ishimoto had the following fatigue properties [39,42]: σ_0 = 233 MPa, τ_0 = 145 MPa, L = 0.246 mm, and m = 1. The sample were tested under proportional (δ = 0°) and non-proportional (δ = 90°) fully-reversed axial loading-torsion by considering different values of nominal biaxiality ratio λ, where $\lambda = \tau_{nom,a}/\sigma_{nom,a}$. As mentioned earlier, the relevant stress fields in the vicinity of the holes were determined by using the analytical solution due to Kirsch [40]. Crack paths were assumed to emanate from the edge of the holes, making angle ζ increase from 0° up to 90° (Fig. 7a). As an example, the charts of Fig. 7b and c show the way both τ_a, ρ_{eff}, and ν_{HSF} vary with angle ζ under both proportional (δ = 0°) and non-proportional

($\delta = 90°$) loading, respectively, the nominal biaxility ratio, λ, being kept constant and equal to 0.5. The above diagrams show that under both $\delta = 0°$ and $\delta = 90°$ the focus path experiencing the largest damage extent was at $\zeta = 35°$ to axis x. Finally, the τ_a vs. ρ_{eff} diagram of Fig. 7d makes it evident that our approach is successful in modelling the detrimental effect of micro-holes, resulting in estimates mainly falling within an error interval of ±20%, this holding true independently from biaxiality ratio, λ, and out-of-phase angle, δ. This clearly confirms that the MWCM applied along with the PM is capable of correctly taking into account the scale effect under multiaxial fatigue loading.

After investigating the accuracy of our approach in designing micro-holes against multiaxial fatigue, attention was focussed on the macro-holed cylindrical samples (Fig. 8a) tested by Gough [6] under in-phase bending and torsion with and without superimposed static stresses. Such specimens were made of S65A, a high-strength steel having the following mechanical/fatigue properties: σ_{UTS} = 1000 MPa, σ_y = 946.3 MPa, σ_0 = 583.5 MPa, τ_0 = 370.5 MPa, m = 0.41, and L = 0.056 mm [6,30]. The stress analysis done using FE software ANSYS® showed that the portion of material subjected to the largest stress was positioned in the vicinity of the junction between the round and internal surface of the hole. Accordingly, as schematically shown in Fig. 8b, the focus paths were assumed to emanate from the curve resulting from the intersection between the round and the hole's surface itself. Fatigue damage was then estimated, for any loading configuration, by exploring focus paths having angle ζ varying in the range 0–50° (see Fig. 8b for the definition of angle ζ). Table 2 shows that, as the degree of multiaxiality of the applied loading changed, the position of the focus path experiencing the largest damage extend varied, the critical path being at $\zeta = 0°$ and $\zeta \approx 43°$ under pure bending and pure torsion, respectively. Finally, both the τ_a vs. ρ_{eff} diagram of Fig. 8c and Table 2 fully confirm that our multiaxial fatigue design methodology was successful also in estimating the detrimental effect of macro-holes, its usage resulting in high-cycle fatigue predictions falling within an error interval of ±20%.

4.4. Cylindrical samples with deep splines under bending and torsion

The technical drawing reported in Fig. 9a shows the geometry of the splined shafts tested by Gough under combined bending and torsion with and without superimposed static stresses. Such shafts were made of S65A, i.e. of the same material as the one used to manufacture the macro-holed samples investigated in the previous section. In order to define the position of those focus paths experiencing the largest fatigue damage extent, the strength analysis was performed by focussing attention on that portion of the critical section reported in Fig. 9b, where the markers denote the origin of the investigated focus paths. Table 3 and the τ_a vs. ρ_{eff} diagram of Fig. 9c show that in the presence of deep splines as well our methodology was capable of high-cycle fatigue estimates falling within an error interval of ±20%, this holding true also under superimposed static stresses.

Turning back to Table 3, we will discuss the calculated positions of the critical locations in more detail. In particular, as to the cracking behaviour of the splined shafts tested under pure bending, Gough himself observes that "... *failure did not occur due to the stress concentration effect of the splined contour*" [6]. Consistently, our approach predicted that, under pure bending, the material experiencing the largest fatigue damage extent was positioned in the vicinity of the upper part of the split contour (points C and D in Fig. 9b). Conversely, under pure torsion as well as under combined bending and torsion, the stress concentration effect was seen to prevail, resulting in critical locations positioned at the end of the bottom fillet (points A and B in Fig. 9c). To conclude, it can be said that the accuracy obtained in predicting the high-cycle fatigue

strength of the splined shaft tested by Gough confirms that our method is capable of performing the fatigue assessment also in those situations in which the position of the critical locations changes significantly as the degree of multiaxiality of the applied load history varies.

4.5. Complex 3D notches subjected to pure bending as well as to combined axial loading and torsion

The validation exercise discussed in the present section involves 3D angular stress concentrators (Figs. 10a and 11a) in which the position of the hot-spot changes as the degree of multiaxiality of the applied loading path varies. Further, for such notches, given the material point experiencing the largest stress magnitude, all the directions emanating from this point experience significant stress gradients.

Initially, the notched square cross-section specimens tested by Bellett et al. [15,41] were considered (Fig. 10a). These samples were made of low-carbon steel En3B (BS040A12) having the following mechanical/fatigue properties [32]: σ_{UTS} = 410 MPa, σ_0 = 273 MPa, τ_0 = 171 MPa, L = 0.2 mm, and m = 1. The above specimens where tested under three-point bending, the point experiencing the maximum stress being the tip of the notch (Fig. 10b).
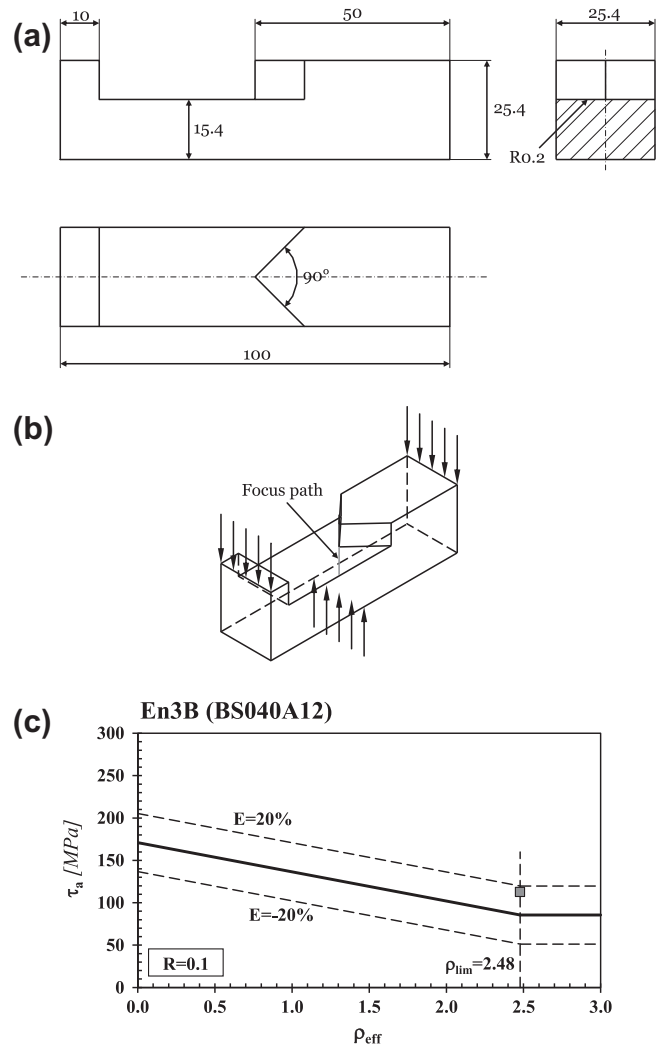

Fig. 10. 3D notch in a square cross-section specimen (a) loaded in three-point bending (b) [15,41], high-cycle fatigue strength estimated according to the MWCM (c).
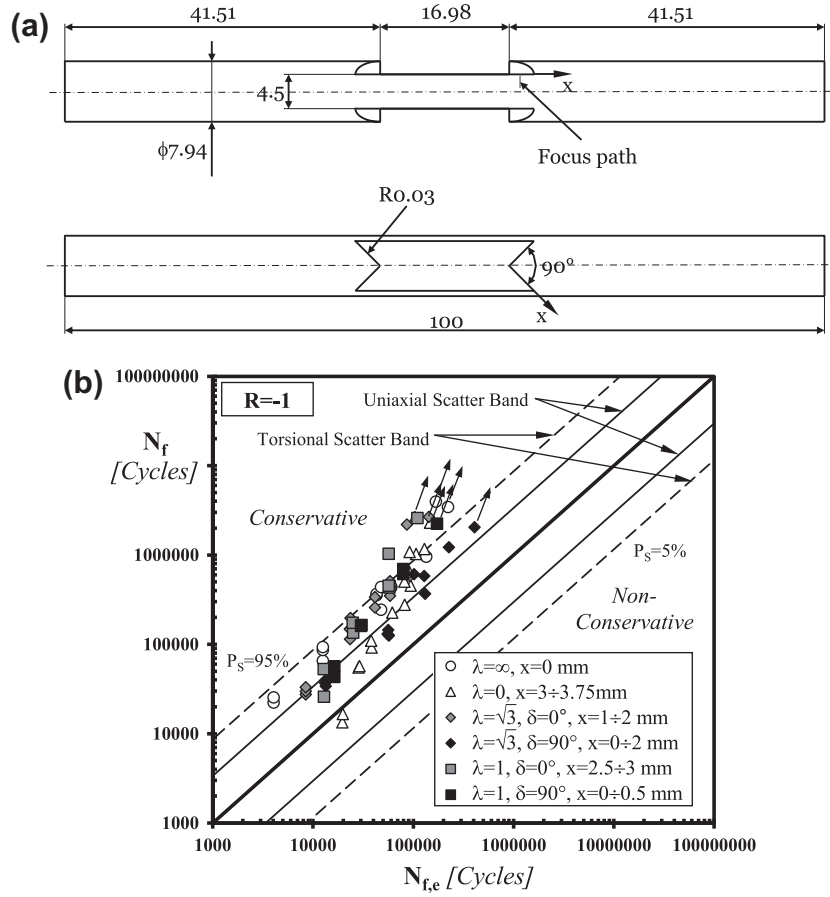
Fig. 11. Cylindrical specimens containing 3D notches and subjected to in-phase and 90° out-of-phase axial loading and torsion (a) [16], finite lifetime estimated according to the MWCM (b).

From close inspection of the geometrical features of the above stress raiser, the hypothesis can be formulated that fatigue cracks initiate at the tip of the notch itself [41]. Accordingly, the focus path was assumed to emanate, at the notch tip, from the end fillet having radius equal to 0.2 mm, such a path being perpendicular to the upper surface of the net section (see Fig. 10b). The τ_a vs. ρ_{eff} diagram of Fig. 10c supports the validity of the assumptions made to define the focus path, the use of our multiaxial methodology resulting in an error of 15.8%.

So far the accuracy of our design method in estimating fatigue damage in the presence of complex 3D stress concentrators has been checked by solely considering high-cycle fatigue situations. For the sake of completeness, the last validation exercise discussed in the present section deals with the finite lifetime problem. In more detail, Capetta et al. [16] tested, under in-phase and 90° out-of-phase axial loading and torsion, cylindrical samples of En3B containing angular notches, the geometry of the investigated notched specimens being sketched in Fig. 11a. For the considered low-carbon steel the MWCM's governing equations as well as the L_M vs. N_f relationship were taken as follows [34]:

$$k_\tau(\rho_{eff}) = 1 \cdot \rho_{eff} + 18.7 \quad (\text{for } \rho_{eff} \leqslant \rho_{lim} = 1.407)$$

$$\tau_{A,Ref}(\rho_{eff}) = -95.3 \cdot \rho_{eff} + 268.3 \quad (\text{for } \rho_{eff} \leqslant \rho_{lim} = 1.407)$$

$$m = 0.22$$

$$L_M(N_f) = 118.9 \cdot N_f^{-0.565}$$

As observed also by Capetta et al. [16], the stress analysis performed using FE software ANSYS® showed that the position of the hot-spot point moved along the bottom edge of the notch as the degree of multiaxiality and non-proportionality of the applied loading changed. Accordingly, the focus paths were assumed to emanate from the end of the fillet, being all perpendicular to the upper surface of the net section (see Fig. 11a). As shown in Fig. 11a, the position of any investigated focus paths was defined through linear coordinate x (having its origin at the notch tip). The experimental, N_f, vs. estimated, $N_{f,e}$, fatigue lifetime diagram of Fig. 11b confirms that our approach was capable of estimates mainly falling, on the conservative side, within the widest scatter band between the two referring to the uniaxial and torsional fully-reversed plain fatigue curves used to calibrate the MWCM itself. This level of accuracy is certainly satisfactory, since we cannot ask a predictive method to be, from a statistical point of view, more accurate than the experimental information used to calibrate the method itself. As shown by the coordinates listed in the legend of Fig. 11b which define the position of the different focus paths used to make the estimates, such a high level of accuracy was obtained by efficiently modelling the fact that the location of the crack initiation point changed as the complexity of the loading path varied [16]. Further, given the profile of the load history, the position of the hot-spot points was seen to slightly vary as the number of cycles to failure changed (see Fig. 11b).

The obtained level of conservatism may be ascribed simply to the fact that, even though they had the same nominal chemical composition and designation, the material used to manufacture

the samples employed to experimentally determine the unnotched fatigue properties [34] and the one used to machine the notched samples whose geometry is sketched in Fig. 11a [16] came from two different batches.

5. Conclusions

(1) The validation exercise reported in the present paper confirms that fatigue strength under uniaxial/multiaxial fatigue loading can accurately be estimated according to the TCD by using that focus path experiencing the largest damage extent.

(2) The MWCM applied along with the PM is seen to be successful in designing metallic components experiencing complex stress concentration phenomena against fatigue, this holding true in the presence of not only non-zero mean stresses, but also non-proportional loading.

(3) Our approach is seen to be capable of accurately modeling the fact that, given the geometry, the position of the critical locations can change as the degree of multiaxiality and nonproportionality of the applied load history varies.

(4) The MWCM used together with the PM is capable of efficiently taking into account the scale effect in fatigue. More work needs to be done instead in order to investigate our method's accuracy in taking into account the volume effect.

(5) The high level of accuracy which was obtained is very promising: the fact that our design approach can be applied by directly post-processing the results from linear-elastic FE models makes it suitable for being used in engineering situations of practical interest.

References

[1] Albert WAJ. Über Treibseile am Harz. Archiv für Mineralogie, Georgnosie. Bergbau and Hüttenkunde 1837;10:215–34.

[2] Wöhler. Versuche zur Ermittlung der auf die Eisenbahnwagenachsen einwirkenden Kräfte und die Widerstandsfähigkeit der Wagen-Achsen. Zeitschrift für Bauwesen 1860;X:583–616.

[3] Spangenburg L. The fatigue of metals under repeated strains. New York, US: D. Van Nostrand Publisher; 1876.

[4] Schütz W. A history of fatigue. Eng Fract Mech 1996;54(2):263–300.

[5] Susmel L. Multiaxial notch fatigue: from nominal to local stress–strain quantities. Cambridge, UK: Woodhead & CRC; 2009. ISBN: 1 84569 582 8.

[6] Gough HJ. Engineering steels under combined cyclic and static stresses. Proc Inst Mech Eng 1949;160:417–40.

[7] Dang Van K, Griveau B, Messagge O. On a new multiaxial fatigue limit criterion: theory and application. In: Brown MW, Miller KJ, editors. "Biaxial and Multiaxial Fatigue", EGF 3. London: Mechanical Engineering Publications; 1989. p. 479–96.

[8] Papadopoulos IV. A high-cycle fatigue criterion applied in biaxial and triaxial out-of-phase stress conditions. Fatigue Fract Eng Mater Struct 1995;18:79–91.

[9] Liu KC. A method based on virtual-strain energy parameters for multiaxial fatigue life prediction. In: McDowell DL, Ellis R, editors. Advances in multiaxial fatigue. Ann Arbor (MI), USA: ASTM STP 1191; 1993. p. 67–84.

[10] Fatemi A, Socie DF. A critical plane approach to multiaxial fatigue damage including out-of-phase loading. Fatigue Fract Eng Mater Struct 1988;11:149–66.

[11] Brown MW, Miller KJ. A theory for fatigue under multiaxial stress–strain conditions. Proc Inst Mech Eng 1973;187:745–55.

[12] Neuber H. Theory of notch stresses: principles for exact calculation of strength with reference to structural form and material. 2nd ed. Berlin: Springer Verlag; 1958.

[13] Peterson RE. Notch sensitivity. In: Sines G, Waisman JL, editors. Metal fatigue. New York: McGraw Hill; 1959. p. 293–306.

[14] Taylor D. The theory of critical distances: a new perspective in fracture mechanics. Oxford, UK: Elsevier Science; 2007.

[15] Bellett D, Taylor D, Marco S, Mazzeo E, Guillois J, Pircher T. The fatigue behaviour of three-dimensional stress concentrations. Int J Fatigue 2005;27(3):207–21.

[16] Capetta S, Tovo R, Taylor D, Livieri P. Numerical evaluation of fatigue strength on mechanical notched components under multiaxial loadings. Int J Fatigue 2011;33(5):661–71.

[17] Susmel L. A simple and efficient numerical algorithm to determine the orientation of the critical plane in multiaxial fatigue problems. Int J Fatigue 2010;32:1875–83.

[18] Susmel L, Tovo R, Socie DF. Estimating the orientation of Stage I crack paths through the direction of maximum variance of the resolved shear stress. Int J Fatigue 2014;58:94–101.

[19] Lemaitre J, Chaboche JL. Mechanics of solid materials. Cambridge, UK: Cambridge University Press; 1990.

[20] Grubisic V, Simbürger A. Fatigue under combined out of phase multiaxial stresses. In: Proceedings of international conference on fatigue testing and design. London: Society of Environmental Engineers; 1976. p. 27.1–8.

[21] Papadopoulos IV. Critical plane approaches in high-cycle fatigue: on the definition of the amplitude and mean value of the shear stress acting on the critical plane. Fatigue Fract Eng Mater Struct 1998;21:269–85.

[22] Li B, Santos JLT, Freitas M. A unified numerical approach for multiaxial fatigue limit evaluation. Mech Struct Mach 2000;28:85–103.

[23] Li B, Santos JLT, Freitas M. A computerized procedure for long-life fatigue assessment under multiaxial loading. Fatigue Fract Eng Mater Struct 2001;24:165–77.

[24] Gonçalves CA, Araújo JA, Mamiya EN. Multiaxial fatigue: a stress based criterion for hard metals. Int J Fatigue 2005;27:177–87.

[25] Zouain N, Mamiya EN, Comes F. Using enclosing ellipsoids in multiaxial fatigue strength criteria. Eur J Mech A/Solids 2006;25:51–71.

[26] Susmel L, Lazzarin P. A Bi-parametric modified Wöhler curve for high cycle multiaxial fatigue assessment. Fatigue Fract Eng Mater Struct 2002;25:63–78.

[27] Lazzarin P, Susmel L. A stress-based method to predict lifetime under multiaxial fatigue loadings. Fatigue Fract Eng Mater Struct 2003;26:1171–87.

[28] Kanazawa K, Miller KJ, Brown MW. Low-cycle fatigue under out-of-phase loading conditions. Trans ASME, J Eng Mater Technol 1977:222–8.

[29] Kaufman RP, Topper T. The influence of static mean stresses applied normal to the maximum shear planes in multiaxial fatigue. In: Carpinteri A, de Freitas M, Spagnoli A, editors. Biaxial and multiaxial fatigue and fracture. Elsevier and ESIS; 2003. p. 123–43.

[30] Susmel L. Multiaxial fatigue limits and material sensitivity to non-zero mean stresses normal to the critical planes. Fatigue Fract Eng Mater Struct 2008;31:295–309.

[31] Susmel L, Tovo R, Lazzarin P. The mean stress effect on the high-cycle fatigue strength from a multiaxial fatigue point of view. Int J Fatigue 2005;27:928–43.

[32] Susmel L, Taylor D. Two methods for predicting the multiaxial fatigue limits of sharp notches. Fatigue Fract Eng Mater Struct 2003;26:821–33.

[33] Susmel L. A unifying approach to estimate the high-cycle fatigue strength of notched components subjected to both uniaxial and multiaxial cyclic loadings. Fatigue Fract Eng Mater Struct 2004;27:391–411.

[34] Susmel L, Taylor D. The Modified Wöhler Curve Method applied along with the theory of critical distances to estimate finite life of notched components subjected to complex multiaxial loading paths. Fatigue Fract Eng Mater Struct 2008;31(12):1047–64.

[35] Susmel L, Taylor D. A critical distance/plane method to estimate finite life of notched components under variable amplitude uniaxial/multiaxial fatigue loading. Int J Fatigue 2012;2012(38):7–24.

[36] Susmel L, Taylor D. A novel formulation of the theory of critical distances to estimate lifetime of notched components in the medium-cycle fatigue regime. Fatigue Fract Eng Mater Struct 2007;30(7):567–81.

[37] Taylor D, Wang G. The validation of some methods of notch fatigue analysis. Fatigue Fract Eng Mater Struct 2000;23:387–94.

[38] Susmel L, Taylor D. Fatigue design in the presence of stress concentrations. Int J Strain Anal Eng Comp 2003;38(5):443–52.

[39] Endo M, Ishimoto I. The fatigue strength of steels containing small holes under out-of-phase combined loading. Int J Fatigue 2006;28:592–7.

[40] Kirsch G. Die Theorie der Elastizität und die Bedürfnisse der Festigkeitslehre. Zeitschrift des Vereins deutscher Ingenieure 1898;42:797–807.

[41] Bellett D. The fatigue behaviour of three-dimensional stress concentrations. PhD Thesis. Dublin, Ireland: Department of Mechanical Engineering, Trinity College; 2002.

[42] Carpinteri A, Montanari L, Spagnoli A, Vantadori S. Size and load effects on the biaxial fatigue resistance of holed structural components. In: Ferro G, Iacoviello F, Susmel L, editors. Proceedings of XXI IGF national conference, Cassino, Italy, 13–15 June 2011. ISBN 978-88-95940-36-6. p. 147–55.